Journal of Solid State Chemistry 181 (2008) 2828–2836

Contents lists available at ScienceDirect

Journal of Solid State Chemistry

journal homepage: www.elsevier.com/locate/jssc

Crystal structure, spectroscopic properties, and magnetic behavior of the fluoride-derivatized lanthanoid(III) *ortho*-oxomolybdates(VI) *Ln*F[MoO_4] (*Ln* = Sm–Tm)

Ingo Hartenbach [a,*], Sabine Strobel [a,b], Peter K. Dorhout [b], Thomas Schleid [a]

[a] *Institut fuer Anorganische Chemie, Universitaet Stuttgart, Pfaffenwaldring 55, D-70569 Stuttgart, Germany*
[b] *Department of Chemistry, Colorado State University, Fort Collins, CO, USA*

ARTICLE INFO

Article history:
Received 13 May 2008
Received in revised form
11 July 2008
Accepted 15 July 2008
Available online 23 July 2008

Keywords:
Oxomolybdates
Lanthanoids
Crystal structures
Magnetic measurements

ABSTRACT

The fluoride-derivatized lanthanoid(III) *ortho*-oxomolybdates(VI) *Ln*F[MoO_4] (*Ln* = Sm–Tm) crystallize in the monoclinic space group $P2_1/c$ with four formula units per unit cell ($a = 516$–528 pm, $b = 1220$–1248 pm, $c = 659$–678 pm, $\beta = 112.5$–113.1°). The structure contains one crystallographically unique Ln^{3+} cation surrounded by two fluoride and six oxide anions in a square antiprism (CN = 8). The square antiprisms [LnF_2O_6] are interconnected via three edges to form layers $^2_\infty\{[LnF^e_{2/2}O^e_{4/2}O^t_{2/1}]^{6-}\}$ parallel (010), which are cross-linked along [010] by Mo^{6+} in tetrahedral oxygen coordination to form the three-dimensional crystal structure. The fluoride anions within this arrangement exhibit a twofold coordination of Ln^{3+} cations in the shape of a boomerang, which is connected to another F^- anion to form planar $[F_2Ln_2]^{4+}$ rhombuses. Magnetic measurements for GdF[MoO_4], TbF[MoO_4], and DyF[MoO_4] show Curie–Weiss behavior, despite the peculiar arrangement of the lanthanoid(III) cations in layers comparable with those of gray arsenic. Furthermore, Raman, infrared, and diffuse reflectance spectroscopy data for these compounds were recorded and interpreted.

1. Introduction

Although, the members of the sixteenth group in the periodic table of the elements, which are mainly *non*-metals, and the sixth group, namely transition metals, do not seem to have many properties in common, some of their compounds are rather comparable. The highest possible oxidation state of chromium, molybdenum and tungsten, is +VI, the same as for sulfur, selenium and tellurium. Whereas sulfur(VI) and selenium(VI), as well as chromium(VI) usually prefer a tetrahedral coordination environment of oxygen atoms, tellurium(VI) is typically sixfold coordinated (e.g. Gd_2TeO_6 [1]). In contrast, molybdenum(VI) and tungsten(VI) are perfectly able to display both, octahedral (e.g. MoO_3 [2] and WO_3 [3]) and tetrahedral coordination environments (e.g. *powellite* Ca[MoO_4] [4] and *scheelite* Ca[WO_4] [5]). While for $[MoO_6]^{6-}$ and $[WO_6]^{6-}$, octahedral edge sharing is generally observed whenever necessary (e.g. in isopolyacids like $H_3(PW_{12}O_{40})$ [6]), the $[MoO_4]^{2-}$ and $[WO_4]^{2-}$ tetrahedra usually remain isolated (e.g. K_2[MoO_4] [7]) or form dimolybdate and ditungstate pyroanions, respectively, by condensation via one single vertex (e.g. $K_2[Mo_2O_7]$ [8]). Higher condensed aggregates like trimolybdate units in $K_2[Mo_3O_{10}]$ [9] or tetramolybdate groups in $K_2[Mo_4O_{13}]$ [10] seem to be built by vertex sharing tetrahedral $[MoO_4]^{2-}$ entities; however, they tend to have one or two additional longer Mo–O distances in order to form trigonal bipyramids $[MoO_{4+1}]^{4-}$ or even octahedra $[MoO_{4+2}]^{6-}$, which are then again connected via common edges, as described before. The most prominent structures with isolated $[MoO_4]^{2-}$ anions are those that crystallize in the *scheelite*-type structure. In order to include lanthanoid(III) cations in this crystal structure, they must share their crystallographic position with equimolar amounts of alkali metal(I) cations (e.g. $NaLaMo_2O_8 \equiv$ (Na,La)[MoO_4] [11]). Another approach to synthesize *ortho*-oxomolybdates(VI) of the trivalent rare-earth elements would be to include an additional monovalent anion X^- into the structure according to the empirical formula *Ln*X[MoO_4]. Thus the lanthanoid(III) fluoride *ortho*-oxomolybdates(VI) *Ln*F[MoO_4] (*Ln* = Sm–Tm) display the first representatives of this new class of compounds.

2. Experimental

2.1. Synthesis

The fluoride-derivatized lanthanoid(III) *ortho*-oxomolybdates (VI) were obtained by the reaction of a mixture of the respective

* Corresponding author. Fax: +49 711 685 54254.
E-mail address: hartenbach@iac.uni-stuttgart.de (I. Hartenbach).

0022-4596/$ - see front matter © 2008 Elsevier Inc. All rights reserved.
doi:10.1016/j.jssc.2008.07.016

lanthanoid trifluoride (SmF_3, EuF_3, GdF_3, TbF_3, DyF_3, HoF_3, ErF_3, TmF_3: all 99.9%; ChemPur, Karlsruhe, Germany), lanthanoid sesquioxide (Sm_2O_3, Eu_2O_3, Gd_2O_3, Dy_2O_3, Ho_2O_3, Er_2O_3, Tm_2O_3: all 99.9%; ChemPur, Karlsruhe, Germany) and molybdenum trioxide (MoO_3: *p.a.*; Merck, Darmstadt, Germany) with the components in the molar ratio of 1:1:3 in evacuated silica ampules for 7 days at 850 °C according to

$$LnF_3 + Ln_2O_3 + 3\ MoO_3 \rightarrow 3\ LnF[MoO_4] \quad (1)$$

Since Tb_2O_3 was not available from commercial sources, it had to be produced *in situ* by the comproportionation of elemental terbium (Tb: 99.9%; ChemPur, Karlsruhe, Germany) and the mixed-valent tetraterbium heptaoxide (Tb_4O_7: 99.9%; ChemPur, Karlsruhe, Germany) in molar ratio of 2:3 according to Eq. (2), in order to obtain $TbF[MoO_4]$.

$$2\ Tb + 3\ Tb_4O_7 \rightarrow 7\ Tb_2O_3 \quad (2)$$

From these reactions transparent, bulky or lath-shaped single crystals emerged, which remained stable in air and water and showed the color of the respective rare-earth metal trication (colorless for *Ln* = Eu, Gd, Tb, Dy, Tm; (pale) yellow for *Ln* = Sm, Ho; pink for *Ln* = Er). Unfortunately, the lanthanoid trifluorides are notorious for attacking the wall of the silica container causing severe contamination of the products with SiO_2, which could be identified via infrared spectroscopy and powder X-ray diffractometry. The product-to-contaminant ratio was about 3:2 considering the cases of $GdF[MoO_4]$, $TbF[MoO_4]$, and $DyF[MoO_4]$, whereas the other reactions showed an even higher level of silicon dioxide in the bulk products, so that only the mentioned three compounds were examined by spectroscopic and magnetic measurements. Attempts to synthesize lanthanoid(III) fluoride *ortho*-oxomolybdates in graphitized silica ampules did not yield better results and the use of refractory metal containers (Nb, Ta) caused the reduction of molybdenum(VI) oxide to molybdenum bronzes with lower oxidation states or to elemental molybdenum.

2.2. X-ray crystallography

The powder X-ray diffraction patterns were measured on a Stoe STADI P diffractometer with a position-sensitive detector using germanium-monochromatized Cu-$K\alpha$ radiation (wavelength: $\lambda = 154.06$ pm). An exemplary powder diffraction pattern of $DyF[MoO_4]$, together with the corresponding theoretical powder pattern was deposited as Supplementary Material. Intensity data sets for single crystals of all $LnF[MoO_4]$ representatives (*Ln* = Sm–Tm) were collected on a Nonius Kappa-CCD diffractometer using graphite-monochromatized Mo-$K\alpha$ radiation (wavelength: $\lambda = 71.07$ pm). Numerical absorption correction was performed with the help of the program HABITUS [12]. The structure solutions and refinements were carried out by using the program package SHELX-97 [13]. Details of the data collections and the structure refinements [14] are summarized in Table 1, atomic positions and coefficients of the isotropic thermal displacement parameters [15] are given in Table 2, interatomic distances and selected bond angles are listed in Table 3, and motifs of mutual adjunction [16] are displayed in Table 4. Further details of the crystal structure investigations are available from the Fachinformationszentrum (FIZ) Karlsruhe, D-76344 Eggenstein-Leopoldshafen, Germany (fax: +497247-808-666; e-mail: crysdata@fiz-karlsruhe.de), on quoting the depository numbers CSD-419247 for $SmF[MoO_4]$, CSD-419248 for $EuF[MoO_4]$, CSD-419249 for $GdF[MoO_4]$, CSD-419250 for $TbF[MoO_4]$, CSD-419251 for $DyF[MoO_4]$, CSD-419252 for $HoF[MoO_4]$, CSD-419253 for $ErF[MoO_4]$, and CSD-419254 for $TmF[MoO_4]$.

2.3. IR spectroscopy

The infrared spectra of $GdF[MoO_4]$, $TbF[MoO_4]$, and $DyF[MoO_4]$ were taken on a Nicolet 6700 FT-IR spectrometer equipped with an ATR unit using a diamond crystal, measuring the reflectance from the powdered samples.

2.4. Raman spectroscopy

The bulk solid-state Raman spectra of $GdF[MoO_4]$, $TbF[MoO_4]$, and $DyF[MoO_4]$ were collected on a Nicolet Magna-IR 760 spectrometer with a FT-Raman Module attachment by use of a Nd:YAG excitation laser (wavelength: $\lambda = 1064$ nm).

Table 1
Crystallographic data for $LnF[MoO_4]$ (*Ln* = Sm–Tm)

	$SmF[MoO_4]$	$EuF[MoO_4]$	$GdF[MoO_4]$	$TbF[MoO_4]$	$DyF[MoO_4]$	$HoF[MoO_4]$	$ErF[MoO_4]$	$TmF[MoO_4]$
Structure parameters	Monoclinic crystal system, space group $P2_1/c$ (no. 14), four formula units per unit cell							
Lattice constants								
a (pm)	527.75(2)	526.09(2)	524.78(2)	522.48(2)	521.21(2)	519.88(2)	518.30(2)	516.18(2)
b (pm)	1248.46(7)	1243.43(7)	1239.26(7)	1234.71(7)	1230.20(7)	1226.98(7)	1223.39(7)	1220.02(7)
c (pm)	678.31(3)	674.97(3)	672.70(3)	669.19(3)	666.41(3)	664.34(3)	661.95(3)	659.28(3)
β (deg)	112.570(2)	112.603(2)	112.744(2)	112.771(2)	112.843(2)	112.956(2)	113.020(2)	113.059(2)
Calculated density D_x ($g\,cm^{-3}$)	5.300	5.392	5.535	5.638	5.759	5.853	5.953	6.049
Molar volume V_m ($cm^3\,mol^{-1}$)	62.132	61.369	60.742	59.928	59.285	58.748	58.160	57.513
$F(000)$	580	584	588	592	596	600	604	608
Index range ($\pm h/\pm k/\pm l$)	6/16/8	6/16/8	6/16/8	6/16/8	6/16/8	6/16/8	6/16/8	6/16/8
Theta range (θ_{min}–θ_{max})	3.26–28.16	3.28–28.28	3.29–28.27	3.30–28.26	3.31–27.48	3.32–28.16	3.33–28.13	3.34–28.22
Absorption coefficient μ (mm^{-1})	17.04	18.23	19.31	20.68	21.92	23.25	24.73	26.26
Data corrections	Background, polarization, and Lorentz factors; numerical absorption correction by the program *HABITUS* [12]							
Reflections, collected/unique	8808/1008	8660/1005	6012/993	7547/978	8946/904	7833/945	5384/926	5690/892
R_{int}/R_σ	0.101/0.037	0.074/0.028	0.070/0.034	0.052/0.023	0.069/0.025	0.087/0.035	0.058/0.032	0.082/0.037
Structure solution and refinement	Program package *SHELX-97* [13]							
Scattering factors	According to International Tables, Vol. C [14]							
R_1 for (♯) reflections with $\lvert F_o\rvert \geqslant 4\sigma(F_o)$	0.021 (982)	0.020 (981)	0.018 (966)	0.020 (950)	0.021 (882)	0.025 (889)	0.023 (849)	0.021 (854)
R_1/wR_2 for all reflections	0.021/0.049	0.021/0.049	0.019/0.038	0.021/0.048	0.022/0.048	0.027/0.060	0.026/0.051	0.022/0.043
Goodness of fit (GooF)	1.073	1.112	1.096	1.074	1.185	1.085	1.045	1.062
Extinction, g	0.0093(4)	0.0423(10)	0.0180(5)	0.0141(5)	0.0115(5)	0.0124(6)	0.0029(4)	0.0108(4)
Residual electron density ρ ($e^- 10^{-6}\,pm^{-3}$), min/max	−1.51/1.56	−1.55/1.61	−1.19/1.28	−1.28/1.26	−1.33/1.81	−1.74/1.76	−1.32/1.50	−1.47/1.57

Table 2
Atomic coordinates and equivalent isotropic thermal displacement parameters U_{eq}[a] for LnF[MoO_4] (Ln = Sm–Tm, all atoms at Wyckoff positions 4*e*)

Atom	*x*/*a*	*y*/*b*	*z*/*c*	U_{eq}
Sm	0.63939(4)	0.44730(2)	0.29874(3)	47(1)
F	0.4479(6)	0.0986(2)	0.0354(4)	127(5)
Mo	0.07741(6)	0.64305(3)	0.13009(5)	49(1)
O1	0.2313(6)	0.3450(3)	0.0849(5)	122(6)
O2	0.1935(6)	0.7731(2)	0.2071(5)	121(6)
O3	0.0090(6)	0.5700(3)	0.3337(5)	97(6)
O4	0.6966(6)	0.0663(2)	0.4619(5)	101(6)
Eu	0.63954(3)	0.44777(1)	0.29885(3)	47(1)
F	0.4485(5)	0.0989(2)	0.0346(4)	120(5)
Mo	0.07705(6)	0.64329(3)	0.12954(5)	47(1)
O1	0.2325(6)	0.3450(3)	0.0862(5)	125(6)
O2	0.1924(6)	0.7737(2)	0.2079(5)	114(6)
O3	0.0077(6)	0.5700(2)	0.3343(5)	94(6)
O4	0.6961(6)	0.0662(2)	0.4599(5)	94(6)
Gd	0.63957(4)	0.44827(1)	0.29906(2)	58(1)
F	0.4492(5)	0.0993(2)	0.0345(3)	122(5)
Mo	0.07733(7)	0.64335(2)	0.12989(5)	59(1)
O1	0.2338(6)	0.3451(2)	0.0876(4)	145(6)
O2	0.1933(6)	0.7744(2)	0.2070(4)	131(6)
O3	0.0075(6)	0.5699(2)	0.3350(4)	102(5)
O4	0.6950(6)	0.0658(2)	0.4603(4)	104(5)
Tb	0.63989(4)	0.44851(2)	0.29922(3)	40(1)
F	0.4505(6)	0.0987(2)	0.0354(4)	108(5)
Mo	0.07730(7)	0.64358(3)	0.12941(5)	40(1)
O1	0.2351(6)	0.3447(3)	0.0889(5)	116(6)
O2	0.1925(7)	0.7747(3)	0.2065(5)	115(6)
O3	0.0053(7)	0.5701(3)	0.3358(5)	91(6)
O4	0.6935(7)	0.0658(3)	0.4623(5)	89(6)
Dy	0.64001(5)	0.44892(2)	0.29921(4)	76(1)
F	0.4518(7)	0.0988(3)	0.0347(5)	142(7)
Mo	0.07710(9)	0.64386(3)	0.12925(7)	75(1)
O1	0.2360(9)	0.3449(4)	0.0911(7)	159(8)
O2	0.1929(9)	0.7756(3)	0.2070(7)	152(8)
O3	0.0057(8)	0.5695(3)	0.3362(6)	116(8)
O4	0.6930(9)	0.0650(3)	0.4614(6)	123(8)
Ho	0.64000(5)	0.44920(2)	0.29937(3)	67(1)
F	0.4544(8)	0.0990(3)	0.0360(6)	136(7)
Mo	0.07754(9)	0.64384(4)	0.12967(7)	68(1)
O1	0.2378(8)	0.3449(4)	0.0922(6)	126(8)
O2	0.1926(9)	0.7764(4)	0.2079(7)	136(8)
O3	0.0050(9)	0.5697(4)	0.3378(6)	110(8)
O4	0.6932(9)	0.0657(4)	0.4624(7)	131(9)
Er	0.64023(5)	0.44955(2)	0.29950(4)	96(1)
F	0.4542(7)	0.0991(3)	0.0353(6)	160(7)
Mo	0.07771(9)	0.64383(4)	0.12968(7)	95(1)
O1	0.2386(8)	0.3449(4)	0.0915(7)	173(9)
O2	0.1934(9)	0.7768(3)	0.2064(7)	165(9)
O3	0.0032(8)	0.5697(3)	0.3361(6)	136(8)
O4	0.6911(8)	0.0651(3)	0.4617(6)	133(8)
Tm	0.64026(4)	0.44975(1)	0.29967(3)	37(1)
F	0.4528(6)	0.0985(2)	0.0346(5)	100(6)
Mo	0.07788(8)	0.64411(3)	0.12935(6)	36(1)
O1	0.2382(8)	0.3456(3)	0.0932(6)	94(7)
O2	0.1940(8)	0.7769(3)	0.2066(6)	110(7)
O3	0.0017(8)	0.5703(3)	0.3380(6)	84(7)
O4	0.6937(8)	0.0645(3)	0.4639(5)	89(7)

[a] $U_{eq} = \frac{1}{3}[U_{22} + \frac{1}{\sin^2\beta}(U_{11} + U_{33} + 2U_{13}\cos\beta)]$ [15].

Table 3
Internuclear distances (*d*/pm, esd = 0.1) and selected bond angles (∠/deg, esd = 0.1) for LnF[MoO_4] (Ln = Sm–Tm)

Ln =	Sm	Eu	Gd	Tb	Dy	Ho	Er	Tm
$[LnF_2O_6]^{11-}$								
Ln–F	227.4	226.0	225.3	224.2	222.8	222.2	221.3	220.4
Ln–F′	233.3	232.6	231.9	230.1	229.5	228.8	228.1	226.5
Ln–O2	235.3	234.5	233.3	232.4	231.0	230.0	228.9	228.2
Ln–O3	241.9	240.0	238.7	236.6	235.1	234.0	232.4	231.1
Ln–O4	242.3	242.3	241.3	238.4	237.8	236.7	235.9	234.4
Ln–O1	244.4	243.2	241.9	240.7	239.3	237.9	237.2	235.8
Ln–O4′	246.4	244.3	242.5	241.3	239.3	239.1	237.0	236.8
Ln–O3′	248.1	246.8	245.3	243.9	242.5	240.8	240.9	239.2
$[MoO_4]^{2-}$								
Mo–O1	172.6	172.4	172.6	172.4	172.6	173.0	172.4	171.9
Mo–O2	174.3	174.1	174.2	173.5	173.7	174.1	173.9	173.3
Mo–O3	180.3	180.6	180.5	181.0	181.0	181.2	180.3	181.0
Mo–O4	181.7	180.6	181.1	181.7	181.8	181.3	181.6	181.1
O1–Mo–O2	106.4	106.5	106.4	106.2	106.5	106.3	106.1	106.6
O1–Mo–O3	106.8	106.6	106.5	106.3	106.4	106.5	105.6	106.0
O1–Mo–O4	106.7	107.1	106.9	106.8	106.7	106.3	107.0	105.6
O2–Mo–O3	113.1	112.8	113.2	113.1	113.3	113.6	113.6	113.9
O2–Mo–O4	113.1	113.5	113.3	113.3	113.6	113.0	113.4	113.2
O3–Mo–O4	110.3	110.0	110.1	110.6	109.9	110.6	110.5	110.8
$[F_2Ln_2]^{4+}$								
F⋯ F	260.7	259.9	259.8	257.4	256.1	255.6	254.9	252.9
Ln⋯*Ln*	379.9	377.9	376.3	374.4	372.9	371.6	370.1	368.4
Ln–F–*Ln*′	111.1	111.0	110.8	111.0	111.1	111.0	110.9	111.1
F–*Ln*–F′	68.9	69.0	69.2	69.0	68.9	69.0	69.1	68.9

Table 4
Motifs of mutual adjunction [16] for LnF[MoO_4] (Ln = Sm–Tm)

	F	O1	O2	O3	O4	CN
Ln	2/2	1/1	1/1	2/2	2/2	8
Mo	0/0	1/1	1/1	1/1	1/1	4
CN	2	2	2	3	3	

2.5. UV–visible spectroscopy

Diffuse reflectance spectra for GdF[MoO_4], TbF[MoO_4], and DyF[MoO_4] have been recorded with a Varian Cary 500 Scan UV–vis–NIR spectrophotometer equipped with a Praying Mantis accessory. A polytetrafluoroethylene standard was used as reference and the Kubelka–Munk function was applied to obtain band-gap information [17].

2.6. Magnetic measurement

Magnetic measurements of GdF[MoO_4], TbF[MoO_4], and DyF[MoO_4] were performed on a Quantum Design SQUID magnetometer. The magnetic susceptibilities were measured at 0.5 T over a temperature range of 1.8–300 K. In addition zero-field cooled (ZFC) and field cooled (FC) data at 0.001 T were collected for all three compounds. Due to the contamination of the three samples with about 40% diamagnetic SiO_2 the calculations for the respective effective magnetic moments and the *Weiss* constants were performed with the assumption that the paramagnetic component LnF[MoO_4] (Ln = Gd, Tb, Dy) comprises 60% of the mass of the weighed sample.

3. Results and discussion

3.1. Crystal structure

The fluoride-containing lanthanoid(III) *ortho*-oxomolybdates (VI) LnF[MoO_4] (Ln = Sm–Tm) crystallize monoclinically in the space group $P2_1/c$ (cell dimensions: a = 516–528 pm, b = 1220–1248 pm, c = 659–678 pm, β = 112.5–113.1°) with four formula units per unit cell; they thus are isotypic with YF[MoO_4]

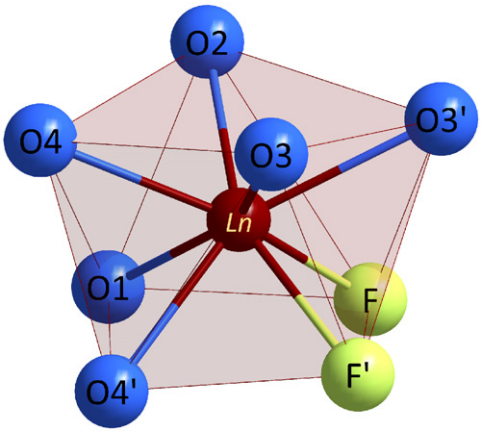

Fig. 1. Coordination polyhedron around the Ln^{3+} cations in the crystal structure of LnF[MoO_4] (Ln = Sm–Tm).

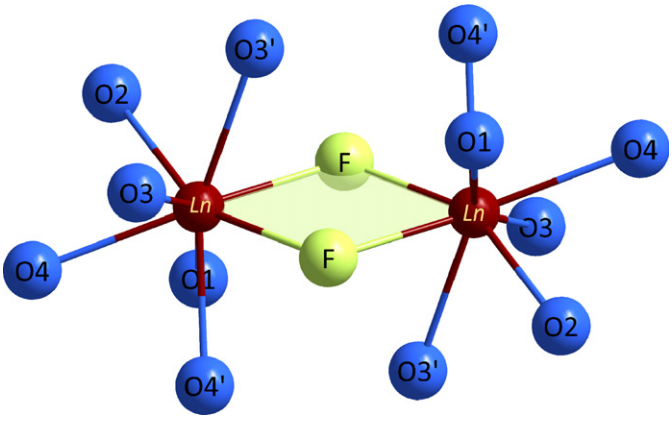

Fig. 2. Planar $[F_2Ln_2]^{4+}$ rhombuses with their surrounding oxygen environment in the crystal structure of LnF[MoO_4] (Ln = Sm–Tm).

[18]. The crystal structure contains one crystallographically unique site for the lanthanoid(III) cations. The coordination sphere around Ln^{3+} is best described as a distorted square antiprism formed by six oxide and two fluoride anions (Fig. 1). The Ln^{3+}–O^{2-} distances cover a range of 235–248 pm for the larger Sm^{3+} and 220–239 pm for the smaller Tm^{3+} cations. These values match rather well those of the respective lanthanoid sesquioxides (B-Sm_2O_3: $d(Sm^{3+}–O^{2-}) = 225–256$ pm [19], C-Tm_2O_3: $d(Tm^{3+}–O^{2-}) = 223–234$ pm [20]). The same is true for the Ln^{3+}–F^- distances with values of 227–233 pm for Ln = Sm and 220–227 pm for Ln = Tm. In the case of Sm^{3+}, these distances compare better with the ternary samarium fluorides ($SmZrF_7$: $d(Sm^{3+}–F^-) = 222–241$ pm [21]) than with the *tysonite*-type SmF_3 ($d(Sm^{3+}–F^-) = 241–247$ pm [22]). The Tm^{3+}–F^- distances also compare very well to those of the respective ternary fluorides ($BaTm_2F_8$: $d(Tm^{3+}–F^-) = 222–231$ pm [23]). Data for the binary TmF_3 are only available by estimating the interatomic distances of TmF_3 in the orthorhombic YF_3-type via shrinking the lattice constants to those determined for TmF_3 [24] and using the atomic positions for YF_3 [24]. This calculation results in distances ranging from 224 to 259 pm, which are also in good agreement with the Tm^{3+}–F^- distances in TmF[MoO_4]. Within this family of solids, the fluoride anions were found to have a coordination number of two in the shape of a boomerang with Ln–F–Ln angles of 111 ± 0.2°. This arrangement, however, does not describe the entire picture, since another fluoride anion connects at the bent side of the fluoride-centered Ln^{3+}-boomerang in order to form the $[F_2Ln_2]^{4+}$ rhombus (Fig. 2). In the solid state, this represents a rather peculiar topology for fluoride anions with CN = 2, since more common arrangements in crystal structures are chains denoted as $^1_\infty\{[FLn_{2/2}]^{2+}\}$, as seen in the analogous lanthanoid(III) fluoride sulfate(VI) GdF[SO_4] [25]. The $F^-\cdots F^-$ distances within these rhombuses range between 253 and 261 pm which is 1–4% higher than the doubled ionic radius of F^- ($r_i(F^-) = 125$ pm [26]). To compensate for the anionic repulsion, the thermal ellipsoids of the fluoride anions show an elongated shape perpendicular to the plane of the rhombus, i.e. due to their polarizability, the F^- anions avoid closer contact to each other by deformation of their electronic shells. The isolated *ortho*-oxomolybdate(VI) $[MoO_4]^{2-}$ entities exhibit a slightly distorted tetrahedral shape (Fig. 3) with Mo^{6+}–O^{2-} bond lengths in the range of 172–182 pm which correspond very well with other rare-earth metal(III) oxomolybdates(VI) (e.g. $La_2[MoO_4]_3$: $d(Mo^{6+}–O^{2-}) = 173–182$ pm [27]), and O–Mo–O angles of 106–114° that are found within ±4° of the ideal tetrahedral angle of 109.5°. In the crystal structure, the square antiprisms $[LnF_2O_6]^{11-}$ form layers parallel to (010) by

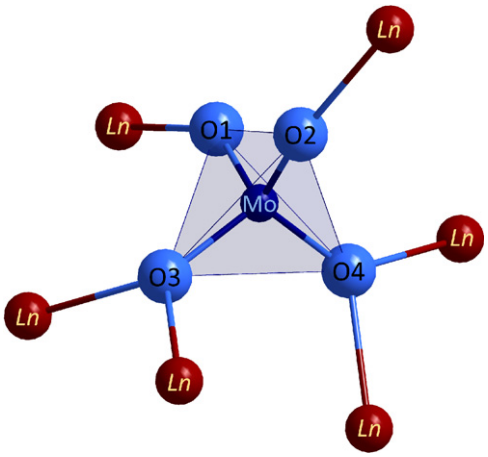

Fig. 3. Tetrahedral $[MoO_4]^{2-}$ anions with their surrounding coordination of lanthanoid cations in the crystal structure of LnF[MoO_4] (Ln = Sm–Tm).

sharing one F···F and two O···O edges according to the scheme $^2_\infty\{[LnF^e_{2/2}O^e_{4/2}O^t_{2/1}]^{6-}\}$. These layers consist of rectangularly shaped voids arranged as seen in Fig. 4 (top). This arrangement can either be described as distorted hexagonal closest packed or as sheared primitive void packing. Along the b-axis these layers are connected by the Mo^{6+} cations in order to form the three-dimensional structure (Fig. 4, bottom). Considering the $[MoO_4]^{2-}$ tetrahedra and the $[F_2Ln_2]^{4+}$ rhombuses as distinct units, each of these lanthanoid fluoride molybdates can be described by the formula $[F_2Ln_2][MoO_4]_2$, which could be related to a common AB_2-type structure. The organization of the above mentioned complex units within the crystal structure results in a ratio of coordination numbers of 12:6 with a hexagonal prismatic environment of B (= $[MoO_4]^{2-}$ units) around A (= $[F_2Ln_2]^{4+}$ units) and a trigonal prismatic coordination of A around B, which may be best described as a distorted AlB_2-type arrangement [28] (Fig. 5). Attempts to extend the domain of existence for this particular structure type to smaller trivalent lanthanoid(III) cations were not successful. The smaller Yb^{3+} and Lu^{3+} cations are obviously not able to maintain a coordination number as high as eight within the "hard" oxide and fluoride anions' coordination environment, nor is Sc^{3+} as the smallest trivalent representative of the rare-earth elements. Attempts to prepare the title compound with ytterbium and lutetium yielded products that could not as yet be clearly identified by powder X-ray diffraction; the scandium

experiments yielded a mixture of unreacted ScF_3 and $Sc_2[MoO_4]_3$ [29], wherein the Sc^{3+} cations are found in octahedral coordination sphere. The same dissatisfying results were obtained for the extension of this new structure type towards the larger lanthanide metals. A coordination number of eight often proves to be insufficient for trivalent lanthanum, cerium, praseodymium and neodymium cations. This finding is supported by the fact, that attempts to synthesize $LaF[MoO_4]$ resulted in the formation of the fluoride-poor compound $La_3F[MoO_4]_4$ [30], in which the La^{3+} cations display a coordination number of nine.

3.2. Infrared and Raman spectroscopy

Both the infrared and the Raman spectra of *Ln*F[MoO_4] were taken from the finely powdered bulk substances, which were contaminated with silicon dioxide (SiO_2) in the β-cristobalite type as confirmed by the powder X-ray diffraction. Thus, broad bands at 1100 and 780 cm^{-1} were observed in the infrared spectra of *Ln*F[MoO_4], which could be assigned to the antisymmetric (1100 cm^{-1}) and symmetric (780 cm^{-1}) stretching vibrations in β-cristobalite-type SiO_2 [31], as seen in Fig. 6 (top) showing the IR-spectrum of $DyF[MoO_4]$ as a representative spectrum. The peaks in the energy range between 980 and 820 cm^{-1} arise from the stretching vibrations of the tetrahedral $[MoO_4]^{2-}$ anions. These vibrations are visible both in the infrared and the corresponding Raman spectrum, wherein the four expected stretching vibrations can clearly be seen between 940 and 750 cm^{-1} (Fig. 6, bottom), of which the largest peak at the highest energy can be assigned to the symmetric and the other three to the antisymmetric stretching vibrations of the oxomolybdate tetrahedra [32,33].

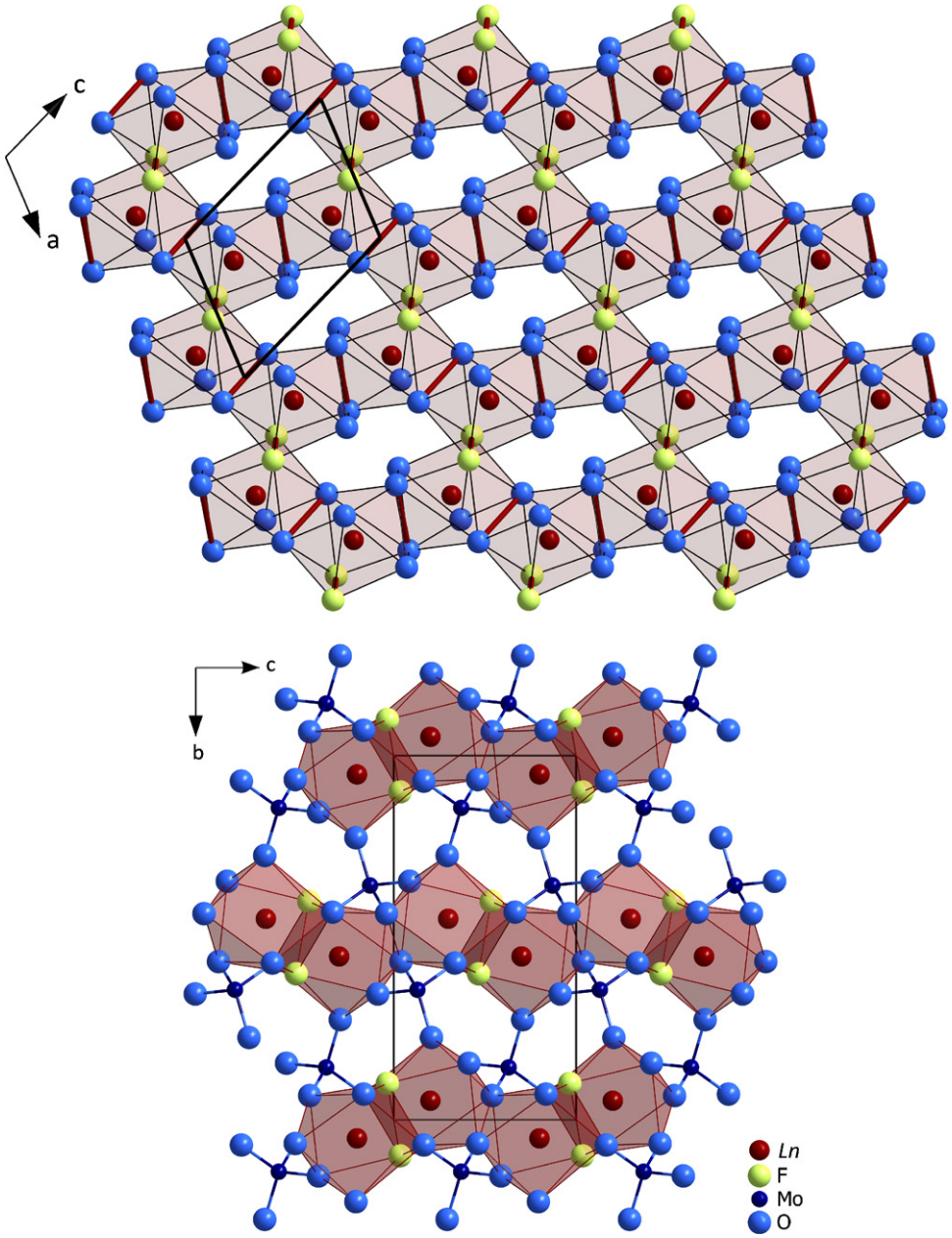

Fig. 4. View at the $^{2}_{\infty}\{[LnF^{e}_{2/2}O^{e}_{4/2}O^{t}_{2/1}]^{6-}\}$ layers parallel (010) (top) and their arrangement in the unit cell (view along the *a*-axis, bottom) in the crystal structure of *Ln*F[MoO_4] (*Ln* = Sm–Tm).

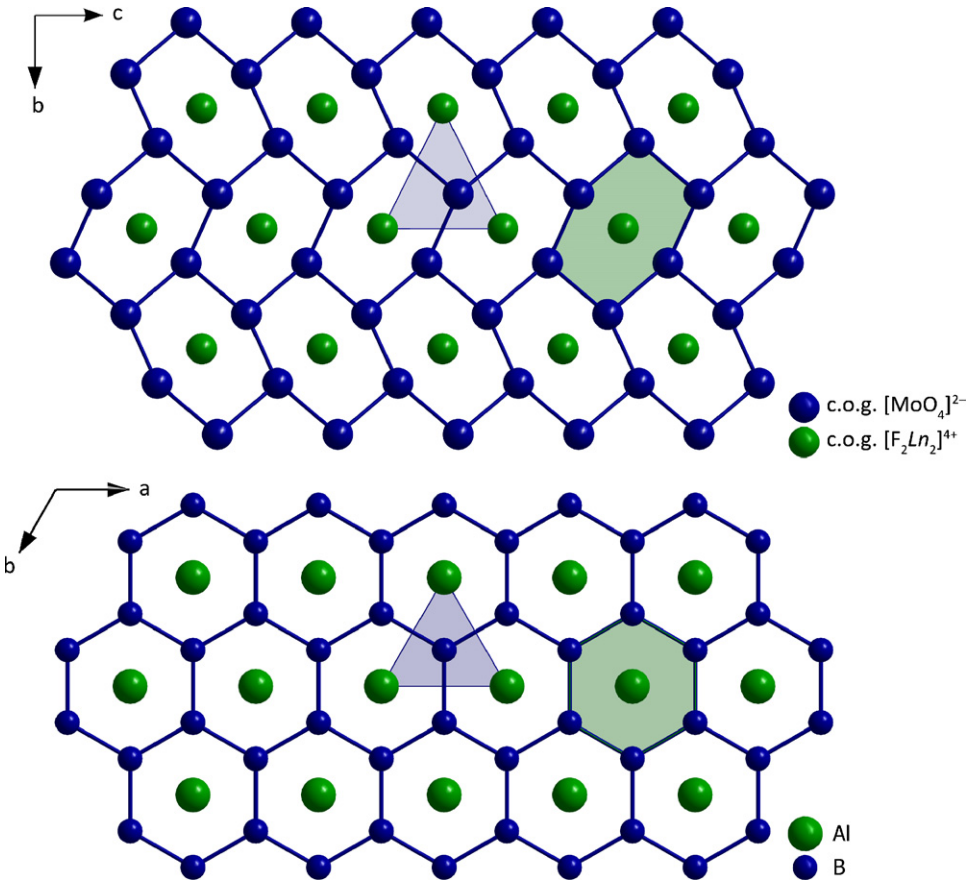

Fig. 5. Comparison of the distorted AlB_2-like arrangement of the centers of gravity (c.o.g.) of the $[MoO_4]^{2-}$ anions and the $[F_2Ln_2]^{4+}$ cations within the crystal structure of LnF[MoO_4] (Ln = Sm–Tm) (top) with the ideal AlB_2 structure (bottom).

The bands of the antisymmetric modes obviously merge into the area of those of β-cristobalite, which can easily be understood since the principle building block of most silicon dioxide modifications is tetrahedral as well ($SiO_2 \equiv {}^3_\infty[SiO^v_{4/2}]$). The deformation vibrations of the $[MoO_4]^{2-}$ anions, however, are situated in the range of 200–400 cm^{-1}, where the Ln–O and Ln–F stretching modes can also be found [34]. Therefore, an explicit assignment of the bands below 400 cm^{-1} is not possible. The same observations are made in the spectra of GdF[MoO_4] and TbF[MoO_4].

3.3. Diffuse reflectance spectroscopy

The diffuse reflectance spectrum of DyF[MoO_4] shows an optical band gap at 3.70 eV, which is situated at 335 nm in the UV range of the electromagnetic spectrum (Fig. 7). Besides the band gap, between 0.6 and 1.7 eV as well as between 2.5 and 3.9 eV $f \rightarrow f$ transitions of the Dy^{3+} cations are also visible. According to [35,36], the peaks in the spectrum of DyF[MoO_4] can be assigned to the transitions as noted in Table 5. The optical band gap in the diffuse reflectance spectrum of GdF[MoO_4] amounts to 3.63 eV (341 nm) while the spectrum of TbF[MoO_4] indicates an optical band gap of 3.61 eV (343 nm).

3.4. Magnetic measurements

The lanthanoid(III) cations in the LnF[MoO_4] structure are aligned in the same layer-like arrangement as the As atoms in the elemental structure of gray arsenic [37] (Fig. 8, top). The interionic distances of Ln^{3+} in the sheets range between 373 and 389 pm (for Ln = Dy) and every line between the lanthanoid(III) cations in Fig. 8 (top), represents a contact of two Ln^{3+} centers through an edge of the respective coordination polyhedron, marked as bold drawn edges in Fig. 4 (top). Because of this special configuration a particular magnetic order could be assumed. However, all the measured compounds show Curie–Weiss behavior at higher temperatures with *Weiss* constants of $\theta_p = -0.5$ K for GdF[MoO_4], $\theta_p = 4.3$ K for TbF[MoO_4], and $\theta_p = 20.5$ K for DyF[MoO_4] (Fig. 8, bottom) without any long range ordering. This fact is also confirmed by the zero-field cooled (ZFC) and field cooled (FC) data at 0.001 T, for which both plots of molar magnetic susceptibility *vs.* temperature are perfectly asymptotic. The deviation from an ideal Curie–Weiss behavior at lower temperatures can probably be assigned to crystal field effects [38]. The experimental effective magnetic moment of DyF[MoO_4] derived from fitting the data to the Curie–Weiss law above 150 K was determined to be 9.71 μ_B, which is about 9% smaller than the theoretical magnetic moment of 10.63 μ_B of Dy^{3+}. This deviation is presumably due to the contamination with diamagnetic SiO_2. Although, a correction of the data as described in the experimental section was performed, the amount of 40% silicon dioxide is probably underestimated. The same correlation was consistently observed for the measured magnetic moments of GdF[MoO_4] and TbF[MoO_4]. With effective magnetic moments of 7.38 μ_B for GdF[MoO_4] (ideal: 7.94 μ_B) and 9.23 μ_B for GdF[MoO_4] (ideal: 9.72 μ_B), which is approximately the same divergence (7% and 5%) as observed for DyF[MoO_4].

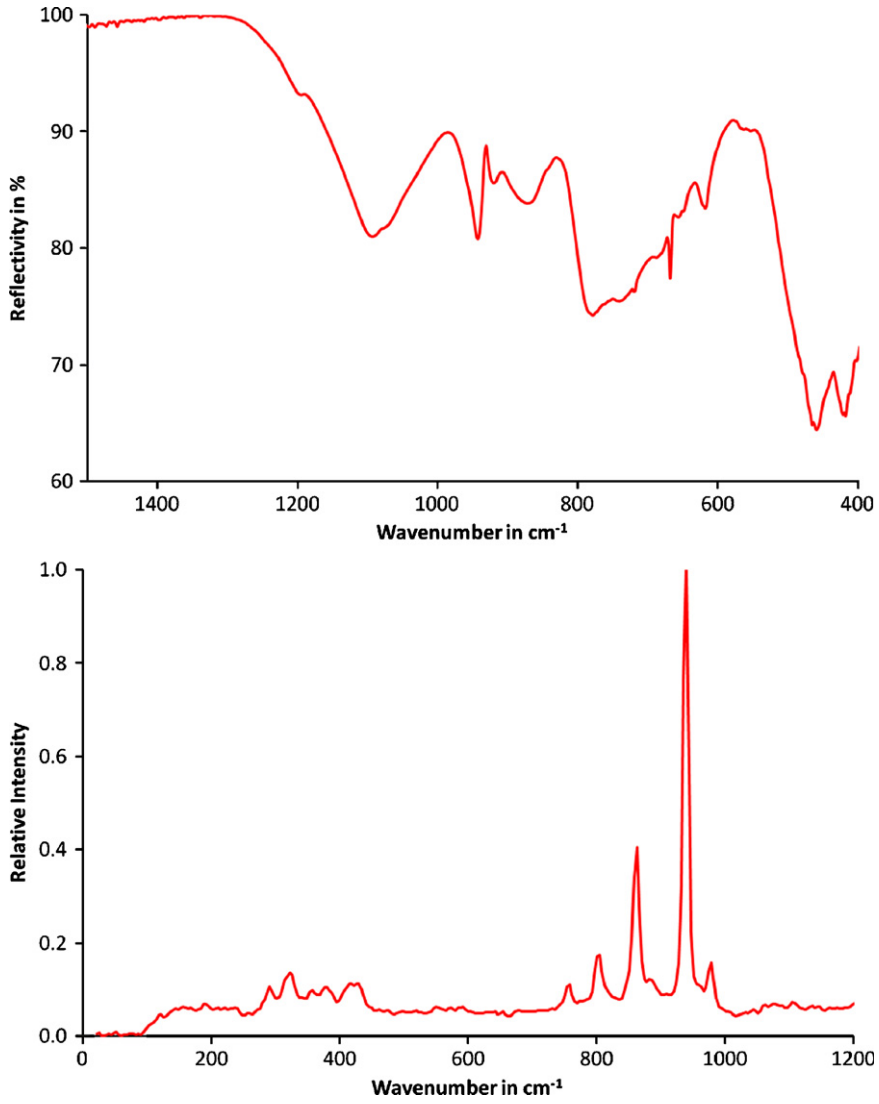

Fig. 6. Infrared (top) and Raman spectrum (bottom) of $DyF[MoO_4]$ as a representative of $LnF[MoO_4]$ (Ln = Sm–Tm).

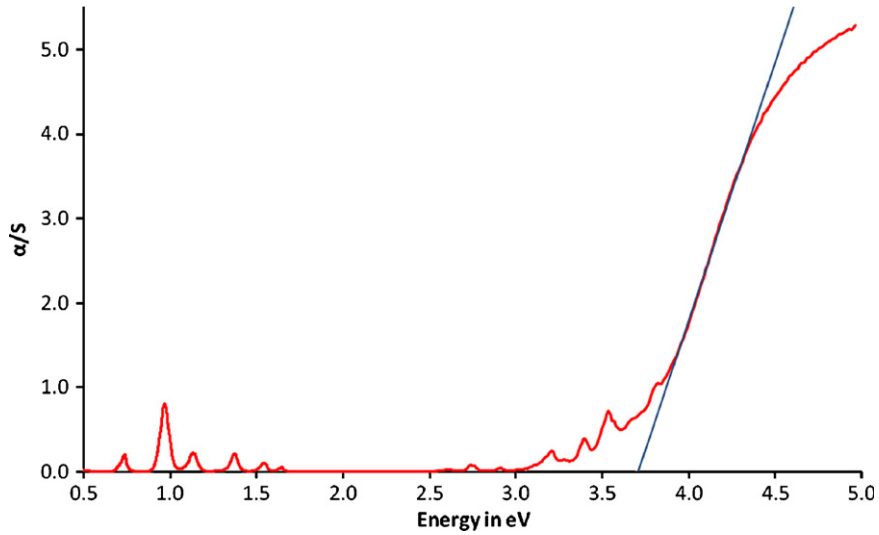

Fig. 7. Diffuse reflectance spectrum of $DyF[MoO_4]$ as a representative of $LnF[MoO_4]$ (Ln = Sm–Tm).

Table 5
Energies of the $f \rightarrow f$ transitions of the Dy^{3+} cations [35,36] in $DyF[MoO_4]$ according to the diffuse reflectance spectrum (Fig. 7)

Energy/eV	Transition from the $^6H_{15/2}$ ground state to	Remarks
0.72	$^6H_{11/2}$	
0.96	$^6F_{11/2}$, $^6H_{9/2}$	
1.11	$^6F_{9/2}$, $^6H_{7/2}$	
1.35	$^6F_{7/2}$, $^6H_{5/2}$	
1.52	$^6F_{5/2}$	
1.61	$^6F_{3/2}$, $^6F_{1/2}$	
2.60	$^4F_{9/2}$	Very weak
2.73	$^4I_{15/2}$	
2.89	$^4G_{11/2}$	
3.19	$^6P_{5/2}$, $^4P_{3/2}$, $^4D_{3/2}$, $^4M_{19/2}$, $^4K_{17/2}$, $^4M_{21/2}$, $^4I_{13/2}$, $^4F_{7/2}$	
3.38	$^4I_{11/2}$	
3.52	$^4M_{15/2}$, $^4I_{15/2}$, $^6P_{7/2}{}^4$	
3.65	$^4I_{9/2}$, $^4F_{5/2}$, $^4D_{5/2}$	Very weak shoulder
3.80	$^4L_{19/2}$, $^4D_{5/2}$, $^6G_{5/2}$, $^4D_{1/2}$, $^4K_{15/2}$, $^6G_{7/2}$, $^2F_{7/2}$, $^4M_{17/2}$, $^6P_{3/2}$,$^4G_{9/2}$	

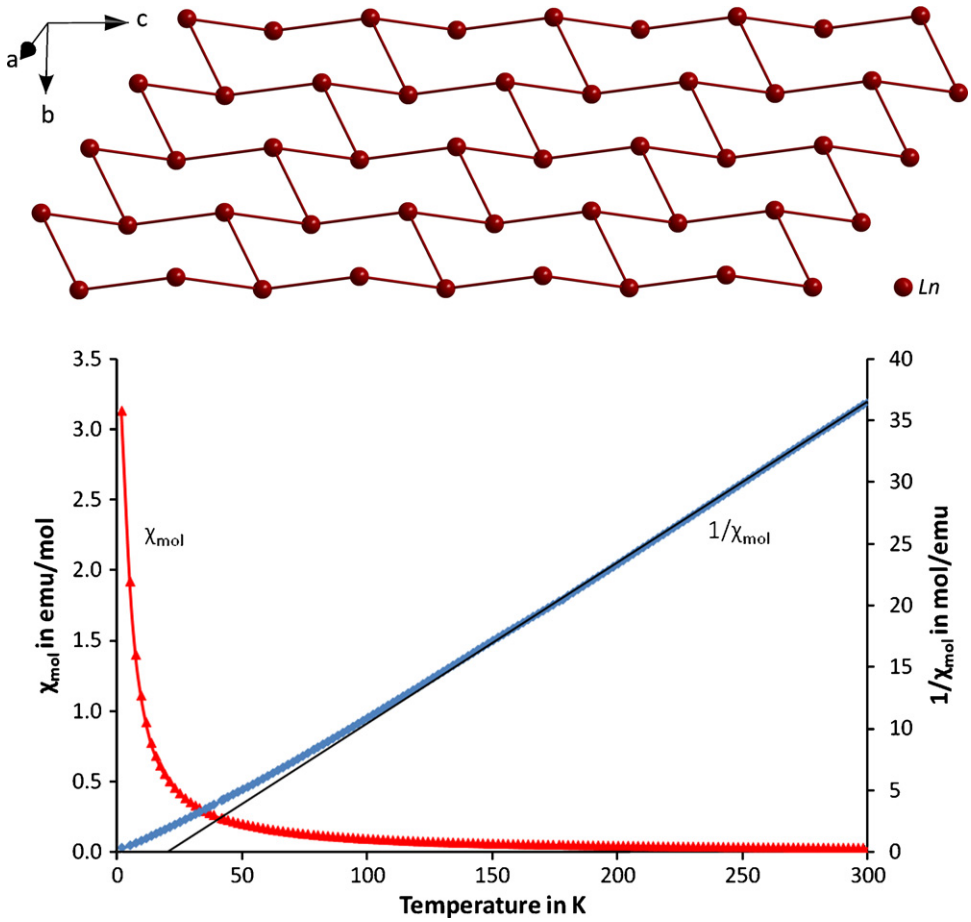

Fig. 8. Layer of lanthanoid(III) cations (top) in the structure of LnF[MoO_4] (Ln = Sm–Tm) exhibiting a topology analogous to the elemental structure of gray arsenic and diagram of the temperature dependence of the molar and inverse molar magnetic susceptibility for DyF[MoO_4] at 0.5 T (bottom). The linear fit to the Curie–Weiss law applies to temperatures above 150 K.

4. Conclusions

In this paper the crystal structure of the lanthanoid(III) fluoride *ortho*-oxomolybdates(VI) is described, along with details of the syntheses and some physical and spectroscopic properties. The crystal structure of this new class of compounds consists of peculiar planar rhombus-shaped $[F_2Ln_2]^{4+}$ units together with twice as many $[MoO_4]^{2-}$ tetrahedra. In the IR spectra, the ranges of the molybdenum–oxygen stretching vibrations were determined and in the Raman spectra they were also assigned to one symmetric and three antisymmetric stretching modes. The optical band gaps of three LnF[MoO_4] representatives (Ln = Gd, Tb, Dy) have been determined. Magnetic measurements were carried out, indicating Curie–Weiss behavior for this class of compounds.

Acknowledgments

We thank Dipl.-Chem. Markus Leboschka and Prof. Dr. Wolfgang Kaim for the collection of the infrared spectroscopic

data. Furthermore, we gratefully acknowledge the financial support of the Deutsche Forschungsgemeinschaft (DFG) within the SPP 1166 "Lanthanoidspezifische Funktionalitäten in Molekül und Material" (Bonn, Germany) and the National Science Foundation (NSF), NSF-DMR-0343412 (Arlington, VA, USA).

Appendix A. Supplementary Materials

Supplementary data associated with this article can be found in the online version at doi:10.1016/j.jssc.2008.07.016.

References

[1] S.F. Meier, Th. Schleid, J. Solid State Chem. 171 (2003) 408–411.
[2] N. Wooster, Z. Kristallogr. 80 (1931) 504–512.
[3] E. Salje, Acta Crystallogr. B 33 (1977) 574–577.
[4] V.B. Aleksandrov, L.V. Gorbatyii, V.V. Ilyukhin, Kristallografiya 13 (1968) 512–513.
[5] A. Zalkin, D.H. Templeton, J. Chem. Phys. 40 (1964) 501–504.
[6] J.F. Keggin, Proc. R. Soc. London Ser. A 144 (1934) 75–100.
[7] B.M. Gatehouse, P. Leverett, J. Chem. Soc. A 1969 (1969) 849–854.
[8] S.A. Magarill, R.F. Klevtsova, Kristallografiya 16 (1971) 742–745.
[9] B.M. Gatehouse, P. Leverett, J. Chem. Soc. A 1968 (1968) 1398–1405.
[10] B.M. Gatehouse, P. Leverett, J. Chem. Soc. A 1971 (1971) 2107–2112.
[11] S.B. Stevens, C.A. Morrison, T.H. Allik, A.L. Rheingold, B.S. Haggerty, Phys. Rev. B: Condens. Matter 43 (1991) 7386–7394.
[12] W. Herrendorf, H. Bärnighausen, HABITUS: program for the optimization of the crystal shape for numerical absorption correction in X-SHAPE (version 1.06, Fa. Stoe, Darmstadt 1999), Karlsruhe, Gießen, 1993, 1996.
[13] G. M. Sheldrick, SHELX-97: Program Package for Solution and Refinement of Crystal Structures from X-ray Diffraction Data, Göttingen, 1997.
[14] Th. Hahn, A.J.C. Wilson (Eds.), International Tables for Crystallography, vol. C, second ed., Kluwer Academic Publishers, Boston, Dordrecht, London, 1992.
[15] R.X. Fischer, E. Tillmanns, Acta Crystallogr. C 44 (1988) 775–776.
[16] C.J.M. Rooymans, A. Rabenau (Eds.), Crystal Structure and Chemical Bonding in Inorganic Chemistry, North-Holland Publishing Company, Amsterdam, 1975, pp. 127–161.
[17] W.W. Wendlandt, H.G. Hecht (Eds.), Reflectance Spectroscopy, Interscience Publishers, New York, 1966.
[18] Th. Schleid, S. Strobel, P.K. Dorhout, P. Nockemann, K. Binnemans, I. Hartenbach, Inorg. Chem. 47 (2008) 3728–3735.
[19] Th. Schleid, G. Meyer, J. Less-Common Met. 149 (1989) 73–80.
[20] W. Hase, Phys. Status Solidi B 3 (1963) K446–K449.
[21] M. Poulain, J. Lucas, J. Solid State Chem. 8 (1973) 132–141.
[22] I. Oftedal, J. Phys. Chem. B 5 (1929) 272–292.
[23] O.E. Izotova, V.B. Aleksandrov, Dokl. Akad. Nauk. SSSR 192 (1970) 1037–1039.
[24] A. Zalkin, D.H. Templeton, J. Am. Chem. Soc. 75 (1953) 2453–2458.
[25] M.S. Wickleder, Z. Anorg. Allg. Chem. 625 (1999) 725–728.
[26] R.D. Shannon, Acta Crystallogr. A 32 (1976) 751–767.
[27] W. Jeitschko, Acta Crystallogr. B 29 (1973) 2074–2081.
[28] W. Hofmann, W. Jaenicke, Naturwissenschaften 31 (1935) 851.
[29] V.A. Efremov, B.I. Lazoryak, V.K. Trunov, Kristallografiya 26 (1981) 72–81.
[30] K. Binnemans, P.K. Dorhout, I. Hartenbach, P. Nockemann, B. Sarkar, Th. Schleid, S. Strobel, Eur. J. Inorg. Chem. (2008), in preparation.
[31] I.P. Swainson, M.T. Dove, D.C. Palmer, Phys. Chem. Miner. 30 (2003) 353–365.
[32] G. Busca, J. Raman Spectrosc. 33 (2002) 348–358.
[33] M. Maczka, K. Hermanowicz, J. Hanuza, J. Mol. Struct. 744–747 (2005) 283–288.
[34] M.M. Lage, A. Righi, F.M. Matinaga, J.-Y. Gesland, R.L. Moreira, J. Phys.: Condens. Matter 16 (2004) 3207–3218.
[35] G.H. Dieke, Spectra and Energy Levels of Rare Earth Ions in Crystals, Interscience Publishers, New York, 1969.
[36] R. Van Deun, K. Binnemans, C. Görller-Walrand, J.L. Adam, J. Alloys Compd. 283 (1999) 59–65.
[37] A.J. Bradley, Z. Kristallogr. 61 (1925) 463–514.
[38] C. Cascales, R. Sáez-Puche, P. Porcher, J. Solid State Chem. 114 (1995) 53–56.